THE JOURNAL OF PHYSICAL CHEMISTRY Letters

Letter

Cite This: J. Phys. Chem. Lett. 2018, 9, 5160−5166

pubs.acs.org/JPCL

Electrochemical Synthesis of Ammonia from N_2 and H_2O under Ambient Conditions Using Pore-Size-Controlled Hollow Gold Nanocatalysts with Tunable Plasmonic Properties

Mohammadreza Nazemi[†,‡] and Mostafa A. El-Sayed*[,†]

[†]Laser Dynamics Laboratory, School of Chemistry and Biochemistry, Georgia Institute of Technology, Atlanta, Georgia 30332-0400, United States

[‡]George W. Woodruff School of Mechanical Engineering, Georgia Institute of Technology, Atlanta, Georgia 30332-0405, United States

Supporting Information

ABSTRACT: An electrochemical nitrogen reduction reaction (NRR) could provide an alternative pathway to the Haber−Bosch process for clean, sustainable, and decentralized NH_3 production when it is coupled with renewably derived electricity sources. Developing an electrocatalyst that overcomes sluggish kinetics due to the challenges associated with N_2 adsorption and cleavage and that also produces NH_3 with a reasonable yield and efficiency is an urgent need. Here, we engineer the size and density of pores in the walls of hollow Au nanocages (AuHNCs) by tuning their peak localized surface plasmon resonance (LSPR); in this way, we aim to enhance the rate of electroreduction of N_2 to NH_3. The interdependency between the pore size/density, the peak LSPR position, the silver content in the cavity, and the total surface area of the nanoparticle should be realized for further optimization of hollow plasmonic nanocatalysts in electrochemical NRRs.

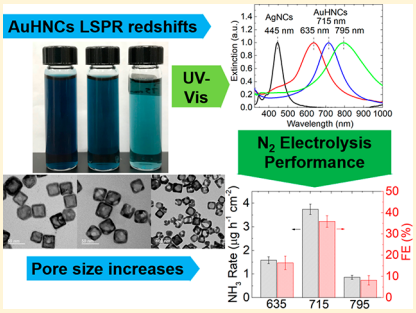

Sustainable ammonia production is vital for global population growth due to ammonia's wide use as a fertilizer in agriculture.[1] The global production of ammonia was 146 million tons in 2015 and is estimated to increase by 40% in 2050.[2,3] Additionally, ammonia, as a carbon-neutral liquid fuel, can be utilized for the development of a clean transportation sector. Ammonia can be used directly in alkaline fuel cells (AFCs) or indirectly as an H_2 source in proton exchange membrane fuel cells (PEMFCs).[4,5] Ammonia can be a substitute for H_2 as a combustion fuel with superior advantages in terms of energy density, ease of liquefaction, and high hydrogen content (i.e., 17.6 wt %). The volumetric energy density of ammonia is 13.6 GJ m^{-3} (~10 atm at 298 K), which is compared with 5.3 GJ m^{-3} for hydrogen at 700 bar pressure.[6]

Conventional ammonia synthesis mainly relies on the Haber−Bosch process, which converts N_2 and H_2 to NH_3 at high operating pressures (150−250 bar) and temperatures (350−550 °C) over iron-based catalysts.[7] The extreme condition requirements for this process necessitate high-cost demands for centralized infrastructure that should be coupled with the global distribution system. Additionally, this process consumes 3−5% of the global natural gas supply and 60% of global hydrogen production and emits 450 million metric tons of CO_2 annually.[8]

As the cost of renewably derived (e.g., solar and wind) electricity continues to decrease given the rapid progress in technology and economies of scale, there is a growing interest in NH_3 electrosynthesis from N_2 and H_2O under ambient conditions. This approach can provide an alternative pathway to the Haber−Bosch process for clean, sustainable, and distributed ammonia synthesis as well as the storage of surplus renewable energy in the form of NH_3 fuel at times of excess supply in the grid.[9,10] Electrification of ammonia synthesis in a large scale requires an effective electrocatalyst that converts N_2 to NH_3 with a high yield and Faradaic efficiency (FE). To date, most studies have shown low electrocatalytic activity and selectivity for NH_3 production mainly due to the high energy required for N≡N cleavage and to competition with the hydrogen evolution reaction (HER).[11−15] Furthermore, the use of molten salt systems and the electrochemical lithium cycling strategy aid in increasing the ammonia yield and FE; however, these strategies are not energetically efficient and require high temperatures (e.g., 450 °C).[16,17] Recently, remarkably higher catalytic efficiency for the electrochemical nitrogen reduction reaction (NRR) was achieved under ambient conditions using various electrocatalytic strategies.[18−22] The main objective of these studies was to improve the selectivity of N_2 on the electrocatalyst's surface by confining N_2 molecules,[20,22] enhancing the electric field at the tip of the electrocatalyst,[18] and using ionic liquid with a specified water content as a proton source.[21]

Received: July 13, 2018
Accepted: August 23, 2018
Published: August 23, 2018

DOI: 10.1021/acs.jpclett.8b02188
J. Phys. Chem. Lett. 2018, 9, 5160−5166

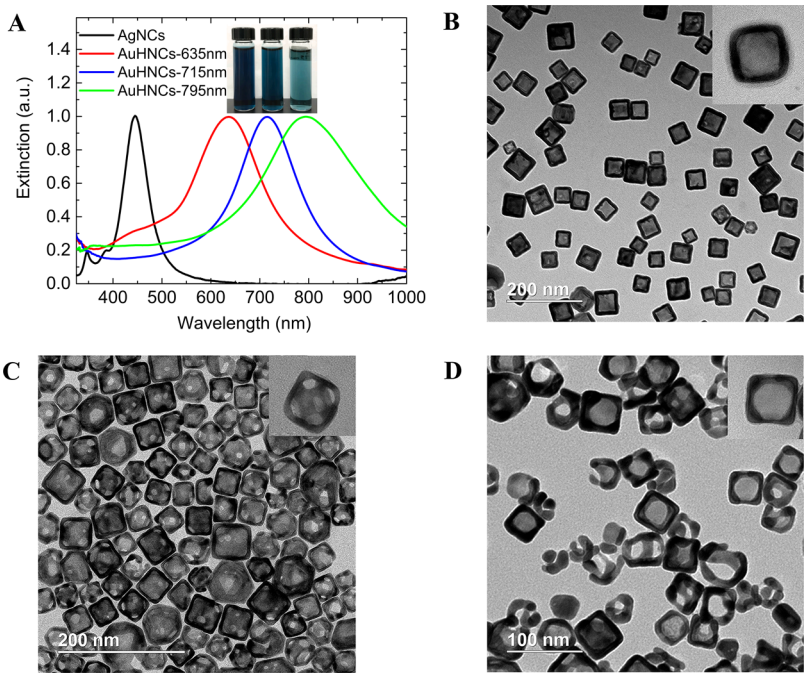

Figure 1. (A) UV−vis extinction spectra of AgNCs and AuHNCs with various peak LSPR values; the photograph shown in the inset is AuHNCs dispersed in DI water. (B−D) TEM images of AuHNCs with peak LSPR values at 635, 715, and 795 nm, respectively. The inset of each image is the magnified TEM image of a nanoparticle.

Table 1. Au and Ag Concentrations and Au and Ag Content (atom %) of Nanoparticles Determined by ICPES[a]

catalyst	Au conc. (μg mL^{-1})	Ag conc. (μg mL^{-1})	Au content (mass %)	Au content[b] (atom %)	ECSA$_{Au}$ (m^2 g^{-1})
AuHNCs-635	1.20	2.44	33.0	21.2	23.4
AuHNCs-715	3.91	3.45	53.1	38.3	26.6
AuHNCs-795	5.40	2.95	64.7	50.1	18.3

[a]The ECSAs of nanoparticles are determined based on the reduction peak of Au oxide during CV measurement in an Ar-saturated 0.1M LiOH solution at a scan rate of 50 mV s^{-1}. [b]The atomic content is calculated using Au and Ag concentrations divided by the molar masses of Au (196.97 g mol^{-1}) and Ag (107.87 g mol^{-1}).

Gold (Au) has been known as one of the best catalysts for the electrochemical NRR through an associative mechanism where breaking of the triple bond of N_2 and hydrogenation of the N atoms occur simultaneously.[23−25] It has been shown that N_2 adsorbs on the Au surface with further hydrogenation to form adsorbed N_2H_x species ($1 < x < 4$), where the rate-determining step is N_2 dissociation (reduction of N_2* to form NNH*).[23,24]

In our previous study, we showed that nanoscale confinement of N_2 enhances selectivity and electrocatalytic activity compared to that of solid Au nanoparticles of various shapes (i.e., cube, sphere, and rod) when the confinement takes place near the electrocatalyst's surface and when it uses hollow Au nanocages (AuHNCs) that have an average edge length of 35 nm and that have peak localized surface plasmon resonance (LSPR) at 660 nm.[22] Here, we aim to find the optimum pore size and density in the walls of AuHNCs in order to further enhance the rate of electroreduction of N_2 to NH_3. This can be accomplished by tuning the peak LSPR of Au nanoparticles. We study the interconnectedness between the pore size/density, the peak LSPR position, the presence of Ag in the interior surface of hollow Au nanostructures, and the active surface area in order to boost the rate of electrochemical NRR.

AuHNCs with various peak LSPR values (i.e., 635, 715, and 795 nm) are prepared by adding hydrogen tetrachloroaurate (0.5 mM $HAuCl_4$(aq)) in solid Ag nanocubes (AgNCs) that are dispersed in DI water using the galvanic synthetic method.[26−28] By increasing the amount of Au^{3+} ions added to the AgNC template with the initial peak LSPR position at 445 nm, the core Ag atoms are etched and the resulting peak LSPR of AuHNCs red shifts (Figure 1A).

The first stage of this synthesis after adding Au^{3+} to the template solution is the formation of nanoboxes with walls composed of Ag−Au alloy at the peak LSPR value of 635 nm (Figure 1B). As more Au^{3+} is added to the boxlike AuHNC solution, the dealloying process of Ag atoms from the Ag−Au walls is initiated. Numerous pores are formed at the walls and corners of AuHNCs at the peak LSPR value of 715 nm (Figure 1C). By further adding Au^{3+} to the porous AuHNCs, the pore size increases while the pore density decreases, and the peak LSPR value red shifts to 795 nm (Figure 1D). By shifting the peak LSPR value from 635 to 715 nm, the small peak at around 445 nm disappears, which indicates the removal of Ag from the interior surface of the cavity (Figure 1A).

The Au and Ag concentrations of all synthesized nanoparticles are determined by inductively coupled plasma emission spectroscopy (ICPES). It is observed that the Au content (mass %) in the nanoparticles increases from 33.0 to 64.7 as the peak LSPR position shifts from 635 to 795 nm (Table 1). In addition, the electrochemical surface areas (ECSAs) of nanocages are determined in the three-electrode setup by performing cyclic voltammetry (CV) in an Ar-

DOI: 10.1021/acs.jpclett.8b02188
J. Phys. Chem. Lett. 2018, 9, 5160−5166

saturated 0.1 M LiOH solution at a scan rate of 50 mV s^{-1}. The $ECSA_{Au}$ is calculated from the reduction peak of Au oxide (~1.2 V vs RHE) after double-layer correction and a charge density of 386 $\mu C\ cm^{-2}_{Au}$ (Figure 2 and Table 1). AuHNCs-715 has the highest $ECSA_{Au}$ (26.6 $m^2\ g^{-1}$), while AuHNCs-795 has the lowest $ECSA_{Au}$ (18.3 $m^2\ g^{-1}$). Although AuHNCs-795 has the highest Au concentration among all nanoparticles (Table 1), it has the lowest $ECSA_{Au}$. This is attributed to the simultaneous reduction of Au and Ag atoms in the final stage of synthesis when the LSPR red shifts from 715 to 795, which changes the porosity of the nanocages and increases the void size. The smaller peak observed for the reduction of Au oxide compared to previous studies[29,30] is due to the significantly smaller Au loading (e.g., 0.19 $\mu g_{Au}\ cm^{-2}_{disk}$ for AuHNCs-715), which is necessary when economic feasibility of using this electrocatalyst for ammonia synthesis is investigated.

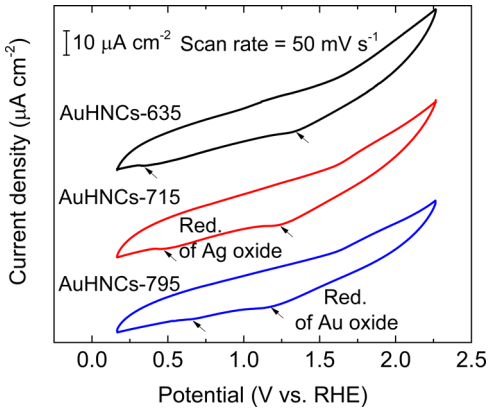

Figure 2. CVs of AuHNCs with various peak LSPR values in an Ar-saturated 0.1 M LiOH aqueous solution at a scan rate of 50 mV s^{-1}. The CV measurements were conducted in the rotating disk electrode (RDE) setup at a rotation rate of 1500 rpm at room temperature. The observed shift in decreasing the reduction potential of Au oxide (~0.15 V) when LSPR red shifts from 635 to 795 nm is attributed to the dealloying process by removal of Ag in the cavity. The second peak in the reduction segment of the CV curve corresponds to the reduction of Ag oxide. The intensity of the peak is proportional to the Ag concentration, which is the highest for AuHNCs-715.

An H-type cell, in which anodic and cathodic compartments are separated by a proton exchange membrane, was set up to carry out electrochemical NRR.[22] The electrolyte is the 0.5 M $LiClO_4$ aqueous solution. Thermodynamically, the NRR occurs at approximately the same potential as the HER (E^0_{RHE} = 0.05 V for NRR and 0 V for HER). Using a Li^+ cation is beneficial due to its strong ability to activate N_2 at ambient conditions and retard the HER process.[14,31] Water oxidation is the primary reaction at the anode, and N_2 gas is purged to the cathode, where the protons produced by water oxidation are transported from the anode to the cathode side through the proton exchange membrane, after which they react with N_2 and produce NH_3.

Linear sweep voltammetry (LSV) tests are carried out in Ar- and N_2-saturated electrolyte to evaluate the selectivity performance ($\frac{I_{N_2} - I_{Ar}}{I_{N_2}} \times 100$) of AuHNCs with various values of peak LSPR toward NRR. The Faradaic current is obtained by subtracting the capacitive current from the actual current recorded from LSV tests. For all electrocatalysts, the current density differs between Ar and N_2 within the potential window of −0.3 to −0.6 V vs RHE (Figure 3A). Beyond this potential window, the HER is the dominant reaction. The highest selectivity toward the NRR (65.3% at −0.4 V vs RHE) is

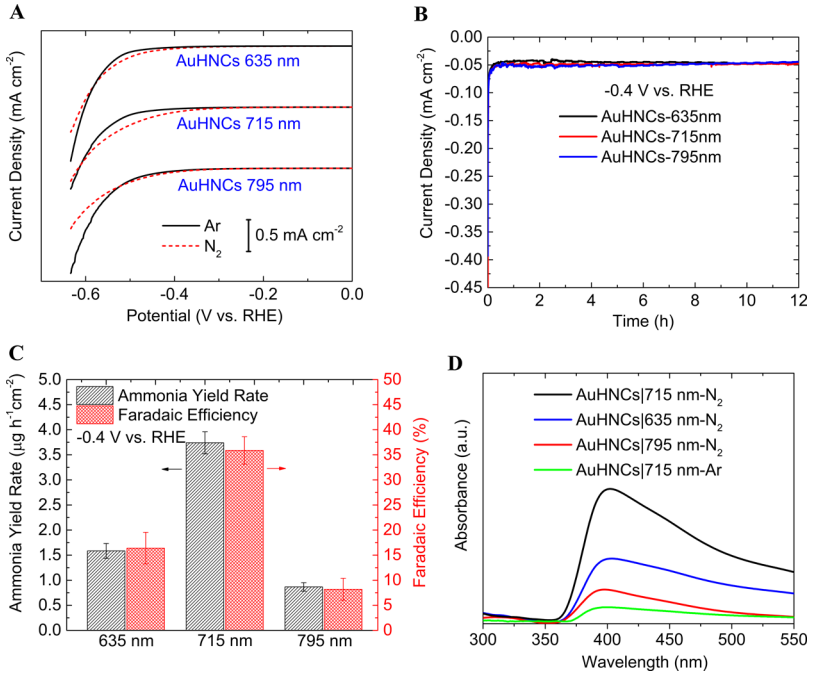

Figure 3. (A) LSV tests of AuHNCs with peak LSPRs at 635, 715, and 795 nm in an Ar- and N_2-saturated 0.5 M $LiClO_4$ aqueous solution under ambient conditions with a scan rate of 10 mV s^{-1}. (B) CA results of AuHNCs with various peak LSPRs at −0.4 V vs RHE in a N_2-saturated 0.5 M $LiClO_4$ aqueous solution. (C) Ammonia yield rate and FE for AuHNCs with various peak LSPR values at a potential of −0.4 V vs RHE in 0.5 M $LiClO_4$. (D) UV−vis absorption spectra of a N_2- and Ar-saturated 0.5 M $LiClO_4$ aqueous solution after electrolysis at −0.4 V vs RHE for 12 h using Nessler's test for AuHNCs with various peak LSPRs.

DOI: 10.1021/acs.jpclett.8b02188
J. Phys. Chem. Lett. 2018, 9, 5160−5166

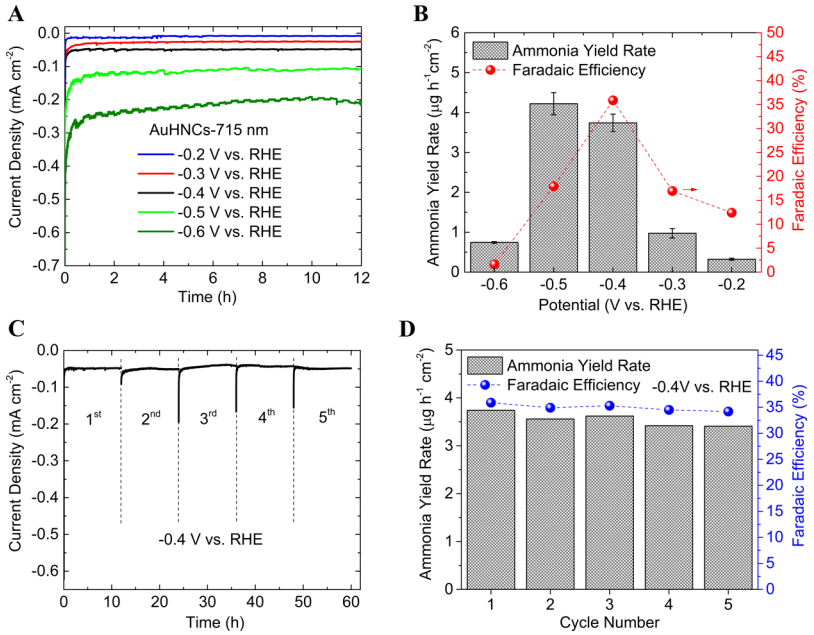

Figure 4. (A) CA results of AuHNCs-715 nm at a series of potentials. (B) Ammonia yield rate and FE at various potentials in a 0.5 M $LiClO_4$ aqueous solution. (C) CA tests for the stability of the AuHNCs-715 nm at −0.4 V vs RHE in a 0.5 M $LiClO_4$ aqueous solution. For each cycle, a CA test was carried out at −0.4 V vs RHE for 12 h. (D) Cycling stability results of the ammonia yield rate and FE on AuHNCs-715 nm. For each cycle, a CA test was carried out at −0.4 V vs RHE in 0.5 M $LiClO_4$.

achieved using AuHNCs-715. This is compared with 48.7 and 27.4% at −0.4 V vs RHE for AuHNCs-635 nm and AuHNCs-795 nm. The complete selectivity performance of electrocatalysts at three different potentials is provided in the Supporting Information (Table S1). The highest N_2 selectivity for AuHNCs-715 is attributed to the compromise between the pore size, the active surface area of the nanoparticle, and the Ag content in the cavity of AuHNCs. Although by increasing the pore size the active surface area of the nanoparticle decreases, the presence of Ag in the cavity of AuHNCs with smaller pore sizes (i.e., AuHNCs-635) decreases the selectivity of an electrocatalyst toward NRR, as Ag enhances H_2 evolution (Table 1). It is noted that all electrochemical experiments are conducted in an O_2-free environment to avoid the formation of Ag_2O in the cavity. As the NRR primarily happens within the cavity, the AuHNCs that have smaller pore size but that have Ag within the cavity (AuHNCs-635) result in lower selectivity for NRR compared with AuHNCs that have bigger pore size but do not have Ag in the cavity (AuHNCs-715). Further increasing the pore size decreases the NRR selectivity due to both the decrease of the surface area and the inefficient confinement of reactants within the cavity (AuHNCs-795). The pore size should be engineered so that reactants can diffuse in and products can diffuse out of the cavity while not losing the surface area notably due to the increase in the pore size in the walls of the nanocages. Therefore, the optimization of the pore size plays a crucial role in confining the reactants in the small region within the cavity and increasing their collision frequency with the interior surface of the electrocatalyst.

Chronoamperomtry (CA) tests are conducted at −0.4 V vs RHE to evaluate electrocatalytic activity and to determine the ammonia yield rate and FE for AuHNCs-635, AuHNCs-715, and AuHNCs-795 (Figure 3B). The highest ammonia yield rate (3.74 $\mu g\ cm^{-2}\ h^{-1}$) and FE (35.9%) are achieved using AuHNCs-715, while the lowest ammonia yield rate (0.87 $\mu g\ cm^{-2}\ h^{-1}$) and FE (8.2%) are obtained for AuHNCs-795 (Figure 3C). This is in line with the trend of the selectivity performance of electrocatalysts for NRR (Figure 3A). A small amount of NH_3 is detected (~0.34 $\mu g\ cm^{-2}\ h^{-1}$, ~9% N_2 gas) when N_2 gas is replaced with Ar under the same applied potential using AuHNCs-715, which indicates that the majority of NH_3 in these experiments originated from the N_2 source (Figure 3D). Hollow Au nanospheres (AuHNSs) with peak LSPR values and electrolysis operating conditions similar to those of AuHNCs (Figure 3C) are evaluated for electrochemical NRR (Figures S2 and S3). The same trend as that for AuHNCs but lower electrocatalytic activity for NRR is observed using AuHNSs. The highest ammonia yield rate (2.77 $\mu g\ cm^{-2}\ h^{-1}$) and FE (29.3%) are achieved using AuHNSs-715; these values are lower than those for AuHNCs-715 (3.74 $\mu g\ cm^{-2}\ h^{-1}$, FE = 35.9%) (Figures S4 and S5). This could be attributed to small variations in the sizes of the nanospheres, cavity volume, pore sizes, and the lack of sharp corners and edges in AuHNSs. The role of pH on the electrocatalytic activity of NRR is evaluated using AuHNCs-715. It is found that operating the N_2 electrolysis in both acidic (0.5 M $LiClO_4$ + 0.001 M $HClO_4$, pH = 3) and alkaline electrolyte (0.1 M LiOH, pH = 13) decreases the rate of ammonia production (Figure S6). This is attributed to the favorable HER in acidic conditions and higher thermodynamic potential for ammonia formation in the alkaline environment ($N_2(g) + 6H_2O + 6e^- \rightarrow 2NH_3(g) + 6OH^-$, $E^0_{RHE} = -0.77$ V). Moreover, decreasing the concentration of Li^+ in the alkaline electrolyte (0.1M) compared with neutral and acidic electrolytes (0.5M) results in a remarkable decrease of the NH_3 yield rate (Table S2). It is noted that an anion exchange membrane (AEM) is used for the electrolysis of N_2 in the alkaline solution to enable the transport of hydroxide anions (OH^-) from the cathode to the anode side for stable electrolysis.

CA tests are performed using AuHNCs-715 to determine the ammonia yield rate and FE at a series of applied potentials (Figure 4A,B). The highest ammonia yield rate (4.22 $\mu g\ cm^{-2}$

DOI: 10.1021/acs.jpclett.8b02188
J. Phys. Chem. Lett. 2018, 9, 5160−5166

h^{-1}) is obtained at −0.5 V vs the RHE with a FE of 17.9%. The higher ammonia yield rate but lower FE at −0.5 V, compared with those at −0.4 V, is due to the compromise between achieving higher current density and higher selectivity toward HER. Moving toward more positive potentials than −0.4 V and more negative potentials than −0.5 V, both the NH_3 yield rate and FE decrease, which is consistent with the LSV results, in which selectivity of the electrocatalyst decreases toward NRR. The stability of AuHNCs-715 is evaluated for 60 h by conducting five consecutive cycles, each for 12 h, at −0.4 V (Figure 4C). The electrocatalyst could maintain continuous NH_3 formation with a stable NH_3 yield rate and FE (Figure 4D). In addition, the SEM images before and after the durability test show that the morphology of supported nanoparticles is reasonably maintanied after 60 h of CA test (Figure S7).

We reported the electrosynthesis of NH_3 from N_2 and H_2O under ambient conditions using AuHNCs with various values of pore size/density by tuning the peak LSPR from 635 to 795 nm. The interdependency between the peak LSPR, Ag content in the interior surface of the hollow Au nanoparticles, pore size/density, and total surface area of the nanoparticle on the electrocatalytic activity of NRR was studied. It was found that the presence of Ag in the cavity for AuHNCs-635 decreases the electrocatalytic activity of NRR. This was attributed to the higher activity of Ag toward HER. Additionally, increasing the pore size by red shifting the peak LSPR value to 795 nm for AuHNCs-795 is not beneficial for increasing the NH_3 yield rate and FE. This is due to the decrease of the active surface area of the nanoparticle and inefficient confinement of reactants in the cavity when the pore size increases. Among all electrocatalysts with various shapes (i.e., cube, sphere) and peak LSPR values (i.e., 635, 715, 795 nm), the highest NH_3 yield rates (3.74 $\mu g\ cm^{-2}\ h^{-1}$) and FE (35.9%) are achieved using AuHNCs-715 at −0.4 V vs RHE.

Although future work requires overcoming the challenge of maintaining a high NH_3 FE at high current densities and suppressing HER, this work leads to empirical structure−activity trends for ammonia synthesis by an array of hollow nanocatalysts with tunable plasmonic properties.

EXPERIMENTAL SECTION

Nanoparticle Synthesis. Preparation of AgNCs and AuHNCs. Silver nanocubes (AgNCs) are prepared by a modified polyol reduction of $AgNO_3$.[32] In a 100 mL round-bottomed flask, 35 mL of anhydrous ethylene glycol (EG) is stirred at 400 rpm and heated at 150 °C for 1 h in an oil bath. After 1 h of heating of the EG, 0.35 g of polyvinylpyrrolidone (PVP, MW ≈ 55 000) dissolved in 5 mL of EG is added at once to the reaction mixture. The temperature of the reaction mixture is then increased gradually until it reaches 155 °C. At this temperature, 0.4 mL of a 3 mM solution of sodium sulfide ($Na_2S.9H_2O$) in EG is added 5 min after the addition of PVP. The solution of sodium sulfide must be prepared 1 h before injection into the reaction mixture. Finally, 0.25 g of $AgNO_3$ dissolved in 5 mL of EG is added at once with stirring set to 200 rpm until the color changes from brownish yellow to pale yellow. Then, the stirring and heating are stopped, and the solution temperature is allowed to decrease to room temperature. To clean the AgNCs solution from the by-products, extra PVP, and organic solvents, 20 mL of the AgNC solution is diluted with 20 mL of acetone and centrifuged for 10 min at 10 000 rpm. The precipitated AgNCs are dispersed in the solution of 0.01 g of PVP dissolved in 100 mL of DI water. To prepare AuHNCs, the cleaned AgNC solution in DI water is heated and brought to boiling. Then, $HAuCl_4$ (0.2 g L^{-1}) in DI water is injected slowly into the AgNCs solution under vigorous stirring (600 rpm) until the peak LSPR spectrum of the solution shifts to the desired value of 635, 715, or 795 nm. The solution is refluxed for 2 min with stirring until the LSPR remains fixed. The solution is cooled down and centrifuged at 10 000 rpm for 10 min. The precipitated nanoparticles are dispersed in DI water for future use.

Preparation of AgNSs. In a 100 mL round-bottom glass flask, 50 mL of EG is stirred and heated at 145 °C for 20 min. Then, 0.4 g of PVP (MW ≈ 55 000) is added to the hot EG. $AgNO_3$ (0.2 g) dissolved in 5 mL of EG is added at once at a stirring speed of 500 rpm. The solution turns yellow due to the reduction of Ag ions into silver nanoparticles. By increasing the time of heating of the solution, the LSPR red shifts and the size of AgNSs increases. The reduction of Ag salt is completed after approximately 7 min. The AgNSs are then quenched using an ice−water solution to avoid increasing the size of AgNSs. The same procedure that was used for AgNCs is used to clean AgNSs.

Preparation of AuHNSs. The precipitated AgNSs are dispersed in a solution of 0.01 g of PVP dissolved in 100 mL of DI water. Then, the solution in water is heated and brought to boiling. $HAuCl_4$ solution (aq, 0.2 g L^{-1}) is injected slowly into the hot Ag solution until the peak LSPR spectrum of the solution shifts to the desired value of 635, 715, or 795 nm. The solution is refluxed with stirring for 2 min until the LSPR becomes fixed. The solution is cooled and cleaned by centrifugation at 10 000 rpm for 10 min. The precipitated nanoparticles are dispersed in DI water for future use.

The AuHNCs with LSPR peaks at 635, 715, and 795 nm have optical densities (ODs) of 1.5, 2.6, and 2.0. The AuHNSs with LSPR peaks at 635, 715, and 795 nm have ODs of 0.8, 1.4, and 1.0.

Determination of the Electrochemical Surface Area (ECSA) of the Nanoparticle. The ECSAs of AuHNCs with various pore sizes were determined by CV tests in an Ar-saturated 0.1 M LiOH aqueous solution (200 mL) in a RDE setup at a rotation rate of 1500 rpm with a scan rate of 50 mV s^{-1}. A polished glassy carbon disk electrode (0.2 cm^2 area) mounted on an interchangeable RDE holder (Pine Instruments) was used as the working electrode. A platinum coil and a single-junction Ag/AgCl reference electrode (4 M KCl with AgCl solution, Pine Instruments) were used as counter and reference electrodes. To mitigate any interferences on CV measurements, both counter and reference electrodes were separated from the main cell by an electrolyte bridge. Prior to measuring CVs for $ECSA_{Au}$ calculation, the working electrode was conditioned by conducting CV tests for 50 cycles at a scan rate of 200 mV s^{-1} to remove possible surface impurities and achieve stable current density response. Then, 20 μL of AuHNCs with 0.1 μL of nafion solution (5 wt %) were sonicated and dispersed on a polished glassy carbon electrode with Au loadings of 0.12, 0.19, and 0.27 $\mu g_{Au}\ cm^{-2}{}_{disk}$ for AuHNCs-635, AuHNCs-715, and AuHNCs-795, respectively. To more uniformly disperse nanoparticles on the glassy carbon, nanoparticles were dried on the glassy carbon with the rotation rate of 600 rpm at room temperature. The $ECSA_{Au}$ of the catalyst was determined from the charge associated with the reduction peak of Au oxide after double-layer correction and was normalized to the Au loading on the working

DOI: 10.1021/acs.jpclett.8b02188
J. Phys. Chem. Lett. 2018, 9, 5160−5166

electrode and a charge density of 386 μC cm^{-2} according to the following equation[33]

$$\mathrm{ECSA}\left(\frac{\mathrm{cm}^2_{\mathrm{Au}}}{\mathrm{g}_{\mathrm{Au}}}\right) = \frac{Q\ (\mu\mathrm{C\ cm}^{-2})}{386\ (\mu\mathrm{C\ cm}^{-2}_{\mathrm{Au}}) \times \text{electrode loading}\ (\mathrm{g}_{\mathrm{Au}}\ \mathrm{cm}^{-2})} \quad (1)$$

where Q (μC cm^{-2}) is the charge associated with the reduction peak of Au oxide after double-layer correction (Figure 2) and calculated according to the following equation

$$Q = \frac{\int iV}{v} \quad (2)$$

where i is the current density (μA cm^{-2}), V is the potential (V), and v (V s^{-1}) is the scan rate.

■ ASSOCIATED CONTENT

Supporting Information

The Supporting Information is available free of charge on the ACS Publications website at DOI: 10.1021/acs.jpclett.8b02188.

Chemicals and materials, electrochemical measurement, working electrode preparation, calibration curves for ammonia quantification, selectivity performance of AuHNCs, calculation of the ammonia Faradaic efficiency, instrumentation, UV−vis and TEM measurements of AuHNSs, NH_3 yield rate and Faradaic efficiency for AuHNSs with various peak LSPR positions, NRR performance with various pH electrolytes using AuHNCs-715, and SEM images before and after the stability test (PDF)

■ AUTHOR INFORMATION

Corresponding Author

*E-mail: melsayed@gatech.edu.

ORCID

Mohammadreza Nazemi: 0000-0002-1735-9277

Mostafa A. El-Sayed: 0000-0002-7674-8424

Notes

The authors declare no competing financial interest.

■ ACKNOWLEDGMENTS

This material is based upon work suppported by U.S. Department of Energy, Office of Basic Energy Sciences, Division of Materials Sciences and Engineering under Award No. DE-FG02-09ER46604 (plasmonic nanostructures with tunable properties) and the National Science Foundation, Division of Chemistry, CHE-1608801 (electrocatalysis). Materials characterization was performed at the Georgia Tech Institute for Electronics and Nanotechnology (IEN), a member of the National Nanotechnology Coordinated Infrastructure, which is supported by the National Science Foundation (Grant ECCS-1542174). The authors are also grateful to Dr. Jeffery A. Donnell for proofreading of the manuscript.

■ REFERENCES

(1) Smil, V. Detonator of The Population Explosion. *Nature* **1999**, *400*, 415.

(2) Survery, U. G. *Mineral Commodity Summaries 2016*; US Geological Survey. US Government Publishing Office: Washington, DC, 2016.

(3) Economic, U. N. D. o.: *World Population Prospects: The 2006 Revision*; United Nations Publications, 2007; Vol. *261*.

(4) Lan, R.; Tao, S. Ammonia as a Suitable Fuel for Fuel Cells. *Front. Energy Res.* **2014**, *2*, 35.

(5) Little, D. J.; Smith, M. R., III; Hamann, T. W. Electrolysis of Liquid Ammonia for Hydrogen Generation. *Energy Environ. Sci.* **2015**, *8*, 2775−2781.

(6) Hua, T.; Ahluwalia, R.; Peng, J.-K.; Kromer, M.; Lasher, S.; McKenney, K.; Law, K.; Sinha, J. Technical Assessment of Compressed Hydrogen Storage Tank Systems for Automotive Applications. *Int. J. Hydrogen Energy* **2011**, *36*, 3037−3049.

(7) Smil, V.: *Enriching the Earth: Fritz Haber, Carl Bosch, and the Transformation of World Food Production*; MIT Press, 2004.

(8) Strait, R.; Nagvekar, M. Carbon Dioxide Capture and Storage in the Nitrogen and Syngas Industries. *Nitrogen+ Syngas* **2010**, *303*, 1−3.

(9) Zamfirescu, C.; Dincer, I. Using Ammonia as a Sustainable Fuel. *J. Power Sources* **2008**, *185*, 459−465.

(10) Klerke, A.; Christensen, C. H.; Nørskov, J. K.; Vegge, T. Ammonia for Hydrogen Storage: Challenges and Opportunities. *J. Mater. Chem.* **2008**, *18*, 2304−2310.

(11) Giddey, S.; Badwal, S.; Kulkarni, A. Review of Electrochemical Ammonia Production Technologies and Materials. *Int. J. Hydrogen Energy* **2013**, *38*, 14576−14594.

(12) Lan, R.; Irvine, J. T.; Tao, S. Synthesis of Ammonia Directly from Air and Water at Ambient Temperature and Pressure. *Sci. Rep.* **2013**, *3*, 1145.

(13) Chen, S.; Perathoner, S.; Ampelli, C.; Mebrahtu, C.; Su, D.; Centi, G. Electrocatalytic Synthesis of Ammonia at Room Temperature and Atmospheric Pressure from Water and Nitrogen on a Carbon-Nanotube-Based Electrocatalyst. *Angew. Chem.* **2017**, *129*, 2743−2747.

(14) Chen, G.-F.; Cao, X.; Wu, S.; Zeng, X.; Ding, L.-X.; Zhu, M.; Wang, H. Ammonia Electrosynthesis with High Selectivity under Ambient Conditions via a Li+ Incorporation Strategy. *J. Am. Chem. Soc.* **2017**, *139*, 9771−9774.

(15) Liu, Y.; Su, Y.; Quan, X.; Fan, X.; Chen, S.; Yu, H.; Zhao, H.; Zhang, Y.; Zhao, J. Facile Ammonia Synthesis from Electrocatalytic N_2 Reduction under Ambient Conditions on N-doped Porous Carbon. *ACS Catal.* **2018**, *8*, 1186−1191.

(16) Licht, S.; Cui, B.; Wang, B.; Li, F.-F.; Lau, J.; Liu, S. Ammonia Synthesis by N_2 and Steam Electrolysis in Molten Hydroxide Suspensions of Nanoscale Fe_2O_3. *Science* **2014**, *345*, 637−640.

(17) McEnaney, J. M.; Singh, A. R.; Schwalbe, J. A.; Kibsgaard, J.; Lin, J. C.; Cargnello, M.; Jaramillo, T. F.; Nørskov, J. K. Ammonia Synthesis from N_2 and H_2O using a Lithium Cycling Electrification Strategy at Atmospheric Pressure. *Energy Environ. Sci.* **2017**, *10*, 1621−1630.

(18) Song, Y.; Johnson, D.; Peng, R.; Hensley, D. K.; Bonnesen, P. V.; Liang, L.; Huang, J.; Yang, F.; Zhang, F.; Qiao, R.; et al. A Physical Catalyst for the Electrolysis of Nitrogen to Ammonia. *Science advances* **2018**, *4*, e1700336.

(19) Mukherjee, S.; Cullen, D. A.; Karakalos, S.; Liu, K.; Zhang, H.; Zhao, S.; Xu, H.; More, K. L.; Wang, G.; Wu, G. Metal-Organic Framework-Derived Nitrogen-Doped Highly Disordered Carbon for Electrochemical Ammonia Synthesis using N_2 and H_2O in Alkaline Electrolytes. *Nano Energy* **2018**, *48*, 217−226.

(20) Lee, H. K.; Koh, C. S. L.; Lee, Y. H.; Liu, C.; Phang, I. Y.; Han, X.; Tsung, C.-K.; Ling, X. Y. Favoring the Unfavored: Selective Electrochemical Nitrogen Fixation Using a Reticular Chemistry Approach. *Science advances* **2018**, *4*, eaar3208.

(21) Zhou, F.; Azofra, L. M.; Ali, M.; Kar, M.; Simonov, A. N.; McDonnell-Worth, C.; Sun, C.; Zhang, X.; MacFarlane, D. R. Electro-Synthesis of Ammonia from Nitrogen at Ambient Temperature and Pressure in Ionic Liquids. *Energy Environ. Sci.* **2017**, *10*, 2516−2520.

(22) Nazemi, M.; Panikkanvalappil, S. R.; El-Sayed, M. A. Enhancing the Rate of Electrochemical Nitrogen Reduction Reaction for Ammonia Synthesis under Ambient Conditions using Hollow Gold Nanocages. *Nano Energy* **2018**, *49*, 316−323.

DOI: 10.1021/acs.jpclett.8b02188
J. Phys. Chem. Lett. 2018, 9, 5160−5166

(23) Yao, Y.; Zhu, S.; Wang, H.; Li, H.; Shao, M. A spectroscopic Study on the Nitrogen Electrochemical Reduction Reaction on Gold and Platinum Surfaces. *J. Am. Chem. Soc.* **2018**, *140*, 1496−1501.
(24) Bao, D.; Zhang, Q.; Meng, F. L.; Zhong, H. X.; Shi, M. M.; Zhang, Y.; Yan, J. M.; Jiang, Q.; Zhang, X. B. Electrochemical Reduction of N_2 under Ambient Conditions for Artificial N_2 Fixation and Renewable Energy Storage Using N_2/NH_3 Cycle. *Adv. Mater.* **2017**, *29*, 1604799−1604804.
(25) Shi, M. M.; Bao, D.; Wulan, B. R.; Li, Y. H.; Zhang, Y. F.; Yan, J. M.; Jiang, Q. Au Sub-Nanoclusters on TiO_2 toward Highly Efficient and Selective Electrocatalyst for N_2 Conversion to NH_3 at Ambient Conditions. *Adv. Mater.* **2017**, *29*, 1606550−1606556.
(26) Sun, Y.; Xia, Y. Shape-Controlled Synthesis of Gold and Silver Nanoparticles. *Science* **2002**, *298*, 2176−2179.
(27) Yen, C.; Mahmoud, M.; El-Sayed, M. Photocatalysis in Gold Nanocage Nanoreactors. *J. Phys. Chem. A* **2009**, *113*, 4340−4345.
(28) Chen, J.; Wiley, B.; Li, Z. Y.; Campbell, D.; Saeki, F.; Cang, H.; Au, L.; Lee, J.; Li, X.; Xia, Y. Gold Nanocages: Engineering their Structure for Biomedical Applications. *Adv. Mater.* **2005**, *17*, 2255−2261.
(29) Zhang, Z.; Xin, L.; Li, W. Supported Gold Nanoparticles as Anode Catalyst for Anion-Exchange Membrane-Direct Glycerol Fuel Cell (AEM-DGFC). *Int. J. Hydrogen Energy* **2012**, *37*, 9393−9401.
(30) Nash, J.; Yang, X.; Anibal, J.; Wang, J.; Yan, Y.; Xu, B. Electrochemical Nitrogen Reduction Reaction on Noble Metal Catalysts in Proton and Hydroxide Exchange Membrane Electrolyzers. *J. Electrochem. Soc.* **2017**, *164*, F1712−F1716.
(31) Suo, L.; Borodin, O.; Gao, T.; Olguin, M.; Ho, J.; Fan, X.; Luo, C.; Wang, C.; Xu, K. Water-in-Salt" Electrolyte Enables High-Voltage Aqueous Lithium-Ion Chemistries. *Science* **2015**, *350*, 938−943.
(32) Mahmoud, M. A.; El-Sayed, M. A. Substrate Effect on the Plasmonic Sensing Ability of Hollow Nanoparticles of Different Shapes. *J. Phys. Chem. B* **2013**, *117*, 4468−4477.
(33) Ralph, T.; Hards, G.; Keating, J.; Campbell, S.; Wilkinson, D.; Davis, M.; St-Pierre, J.; Johnson, M. Low Cost Electrodes for Proton Exchange Membrane Fuel Cells Performance in Single Cells and Ballard Stacks. *J. Electrochem. Soc.* **1997**, *144*, 3845−3857.

DOI: 10.1021/acs.jpclett.8b02188
J. Phys. Chem. Lett. 2018, 9, 5160−5166